NJC

Accepted Manuscript

This is an *Accepted Manuscript*, which has been through the Royal Society of Chemistry peer review process and has been accepted for publication.

Accepted Manuscripts are published online shortly after acceptance, before technical editing, formatting and proof reading. Using this free service, authors can make their results available to the community, in citable form, before we publish the edited article. We will replace this *Accepted Manuscript* with the edited and formatted *Advance Article* as soon as it is available.

You can find more information about *Accepted Manuscripts* in the **Information for Authors**.

ROYAL SOCIETY OF CHEMISTRY

www.rsc.org/njc

Photoelectrochemical Activity and Its Mechanism of Mesoporous TiO$_2$ Nanotube Arrays Prepared with Chemical Etching Method

Jinwen Wang[1], Guangqing Xu[*1, 2], Xu Zhang[1], Jun Lv[1], Dongmei Wang[1], Zhixiang Zheng[1], Jianmin Wang[1], Yucheng Wu[*1, 2]

1 School of Materials Science and Engineering, Hefei University of Technology, Hefei 230009, China

2 Anhui Provincial Key Laboratory of Advanced Functional Materials and Devices, Hefei University of Technology, Hefei 230009, China.

Abstract: Novel mesoporous TiO$_2$ nanotube arrays were synthesized by anodization method combined with chemical etching method for enhancing the photoelectrochemical activity. Morphologies, structures and elemental compositions of mesoporous TiO$_2$ nanotube arrays were characterized with scan electron microscope, high resolution transmission electron microscope, X-ray diffraction and X-ray photoelectron spectroscopy. Photoelectrochemical property was measured with cyclic voltammetry and chronoamperometry using an electrochemical workstation equipped with a UV LED light (365 nm). Higher photoelectrochemical activities of mesoporous TiO$_2$ nanotube arrays can be achieved with the highest photocurrent triple that of un-etched TiO$_2$ nanotube arrays. High electrochemical active surface area, optical absorption ability and charge transfer rate play key roles on enhancing the photoelectrochemical activity of mesoporous TiO$_2$ nanotube arrays.

Keywords: TiO$_2$ nanotube arrays; Mesoporous structure; Chemical etching; Photoelectrochemical activity

1 Introduction

As one of semiconductors, TiO$_2$ has received wide attention since 1972 when Fujishmia and Handa [1-3] discovered photocatalytic splitting of water on a TiO$_2$ electrode under ultraviolet (UV) light. And it is widely used in dye-sensitized solar cells [4-6], photocatalysis [1-3], ion-intercalation devices [7-9] and sensors [10-12], due to its nontoxicity, photocorrosion free, physical and chemical stability. Well aligned TiO$_2$ nanotube arrays (NTAs) were synthesized by Grimes via anodizing Ti sheets in HF solution [13]. Such ordered TiO$_2$ NTAs offer high surface areas, well-defined nanostructure, favorable transport pathways and good adhesion to the substrate. The vertically oriented TiO$_2$ NTAs became a competing substrate in functional devices, including COD sensors

---

* Corresponding author: Tel.: +86 551 62901372
Email address: gqxu1979@hfut.edu.cn (Guangqing Xu)
                ycwu@hfut.edu.cn (Yucheng Wu)

[14-16], Li-ion batteries [17-19], CO_2 reduction and water splitting [20-22].

There are two shortcomings restraining the further applications of TiO_2 nanomaterials. First, an inefficient harvest of solar energy due to its wide band gap of 3.2 eV. Second, a relatively high recombination rate of the photogenerated electron-hole pairs in the charge transfer process. Hence, many efforts have been endeavored to address these two bottlenecks by surface modifications including metal nanoparticles [23, 24] and narrow band gap semiconductors [25-27]. These modifications enhance the photocatalytic properties by controlling charger transfer in the external surface of TiO_2 nanomaterials. The internal structure of TiO_2 is the other key factor for photocatalysis, including the crystal structure, geometric dimensions and the surface condition. For example, the different exposed lattice planes of TiO_2 nanocrystals possess different catalytic reaction activity [28].

A lot of efforts have been dedicated to synthesize TiO_2 nanomaterials with a controllable morphology and porous structure [29]. In particular, mesoporous TiO_2 not only increases surface area but also facilitates the transfer of photogenerated chargers, resulting in efficient optical harvesting, high surface reaction activity and low charge transfer resistance, hence enhancing the photocatalytic and photoelectrochemical properties. Bao and co-workers first developed a novel TiO_2 with a uniform porous structure via multi-walled carbon nanotubes as templates [30]. Jaturong Jitputti et al. synthesized mesoporous TiO_2 by hydrothermal method for water splitting [31]. Pascal Hartmann et al. found that mesoporous TiO_2 films caused an about 10 times higher efficiency for the water splitting reaction than TiO_2 nanoparticles [32]. These results confirm the efficiency of mesoporous structure on photocatalytic properties of TiO_2.

Considering the synthesis process of anodized TiO_2 NTAs, chemical etching is an easy method for constructing mesopores in TiO_2 nanotubes, which can remain the well aligned array structures. To our knowledge, the introduction of mesopores in TiO_2 NTAs for enhancing the photoelectrochemical property has never been reported. Here, TiO_2 NTAs with mesoporous structures are obtained by anodization method combined with chemical etching in HF solution. The mechanism of mesoporous structures on enhancing photoelectrochemical property of TiO_2 NTAs is deeply discussed.

2 Prefer Experimental

2.1 Chemicals and instruments

Chemicals, such as Ethylene glycol (EG), disodium hydrogen phosphate (Na_2HPO_4), sodium dihydrogen phosphate (NaH_2PO_4), ammonium fluoride (NH_4F), hydrogen fluoride (HF) and other

reagents were in analytical reagent grade and purchased from Enterprise group chemical reagent Co, LTD. Titanium foils with a thickness of 0.1 mm (99.7% purity) were purchased from Beijing Cuibolin Non-Ferrous Technology Developing Co. LTD and used as received. A 0.05 M phosphate buffer solution (pH=7) consisting of Na_2HPO_4 and NaH_2PO_4 was used as supporting electrolyte in photoelectrochemical measurements.

Anodization of TiO_2 NTAs was conducted in a self-made electrolytic cell with a voltage-stabilized source (DH1722A-3). The anodized TiO_2 NTAs were in amorphous structure and crystallized in a muffle furnace (OTF-1200X). Morphologies of the as-prepared samples were observed with scanning electron microscope (SEM, SV8020) and high resolution transmission electron microscope (HRTEM, JEM-2100F). X-ray diffraction patterns of the samples were recorded at room temperature with 2θ angle ranging from $10°$ to $80°$ (XRD, D/MAX2500V). The existence valence of TiO_2 NTAs was determined by X-ray photoelectron spectrometer (XPS, CALAB250).

All electrochemical experiments were performed on a CHI 660D electrochemistry workstation (Chenhua instrumental Co., LTD. Shanghai, China), comprising three electrodes of an Ag/AgCl (3 M KCl) reference electrode, a platinum wire auxiliary electrode and a TiO_2 NTAs working electrode (diameter of 10 mm). The photoelectrochemical properties were measured on the workstation equipped with a UV LED spot source with a maximum optical power of 1200 mW/cm^2, wavelength of 365 nm and spot diameter of 10 mm. The optical power can be adjusted by controlling the electric powers outputs from 0 to 100%. The absorption spectra of samples were analyzed by UV-Vis scanning spectrophotometer (Shimadzu UV-3600).

2.2 Synthetic procedure

Ti foil was ultrasonically rinsed in acetone and ethanol for each 15 min prior to anodization. Ti foil was put into a two-electrode electrolytic cell as the working electrode, and a graphite electrode was used as the counter electrode. The distance between the two electrodes was 2 cm. Highly ordered TiO_2 NTAs were prepared by anodic oxidation in EG solution containing 0.15 M NH_4F and 5% H_2O at the voltage of 60 V for 6 h. Then, the anodized TiO_2 NTAs were ultrasonic vibrated in EG for 1 min to remove the broken nanotubes covered on top surface of TiO_2 NTAs. The dried TiO_2 NTAs were annealed in a muffle furnace at 500℃ for 2 h to get anatase TiO_2 NTAs.

The mesoporous structure of TiO_2 NTAs were constructed by chemical etching method in HF solution with 0.5:10:89.5 volume ratio of HF, H_2O to EG. 6 mL as-prepared solutions were transferred to a Teflon-lined stainless steel autoclave containing the anatase TiO_2 NTAs inside. Then

the autoclaves were sealed and maintained at 100℃, 140℃, 180℃ and 200℃ for 5 h, respectively, to complete the chemical etching process. Then the products were rinsed in deionized water several times and dried at the room temperature. For comparison, TiO_2 NTAs without chemical etching were also prepared. The samples are defined as TiO_2-n, where n is the hydrothermal temperature.

2.3 Photoelectrochemical property

All the photoelectrochemical properties were measured in a self-made flow-injection photoelectrochemical cell equipped with a UV LED spot source with wavelength of 365 nm, spot diameter of 10 mm and adjustable optical powers ranging from 0 to 1200 mW/cm^2.

Cyclic voltammetry with potentials ranging from 0 to 1 V and sweeping rate of 10 mV/s, was used to characterize the photoeletrochemical activities of different TiO_2 NTAs in phosphate buffer solution in dark and under illumination, respectively. Photocurrents of TiO_2 NTAs were measured by chronoamperometry with an applied potential of 0.2 V in phosphate buffer solution. The light was switched on and off at an elapse of 100 s. The increment of currents before and after the UV light illumination gave the photocurrent due to the photocatalytic reaction of water splitting.

3 Results and discussion

3.1 Characterization of mesoporous TiO_2 NTAs

It is well established that the crystallinity of TiO_2 plays an essential role in the phototcatalytic activity. TiO_2 with poor crystallinity, such as amorphous TiO_2, normally possess low photocatalytic activity due to the severe structure defects act as the recombination centers of photogenerated electrons and holes [33]. A simple calcination process at a high temperature is an effective way to realize the crystallization of TiO_2 semiconductor.

Fig.1 shows XRD patterns of TiO_2 NTAs and mesoporous TiO_2 NTAs with different etching temperatures ranging from 100 to 200℃. The diffraction peaks at 25.28° and 37.8° correspond to the (101) and (004) lattice planes of anatase TiO_2, indicating that TiO_2 NTAs are in anatase structure after being annealed, as shown in curve (a) of Fig.1. The diffraction peak at 40.17° corresponds to the lattice plane (101) of substrate Ti. The XRD pattern of mesoporous TiO_2-100 NTAs is almost the same with that of un-etched TiO_2 NTAs, as shown in curve (b) of Fig.1, indicating that the chemical etching in 100℃ has no influence on the crystal structure of TiO_2 NTAs. The further increase of the etching temperature change the XRD patterns a little in the background. Although the same diffraction peaks in all TiO_2 NTAs manifest there is no change in the main structure after being etched, high diffraction backgrounds in curve (c), (d) and (e) indicate the change on the surface of

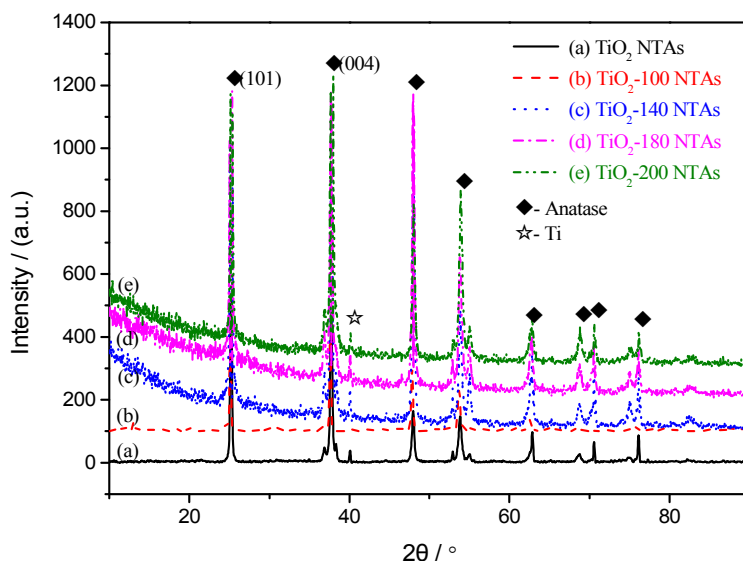TiO$_2$ nanotubes, which may be due to the surface structures with low crystallinity.

Fig.1 XRD patterns of TiO$_2$ NTAs and mesoporous TiO$_2$ NTAs with different etching temperatures

The commonly used XPS is applied to identify the elemental chemical state in TiO$_2$ NTAs and mesoporous TiO$_2$ NTAs, as shown in Fig.2. Fig.2 (i) shows the survey patterns of TiO$_2$ and mesoporous TiO$_2$-180 NTAs. Sharp peaks of O1s and Ti2p at 530.02 eV and 458.45 eV detected in both samples confirm the major ingredients of the samples. Peak of C1s at 284.8 eV, found in both patterns, is originated from the texting process of XPS. Peak at 684.2 eV corresponding to F$^-$ ions may originate from the anodization process or the chemical etching process. The survey pattern of TiO$_2$-180 NTAs is almost the same to that of un-etched TiO$_2$ NTAs.
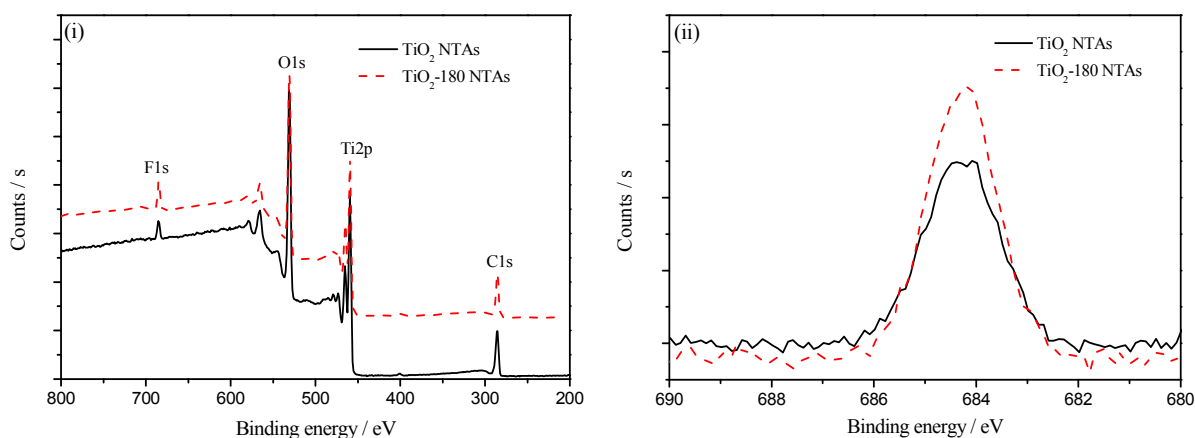

Fig.2 XPS patterns of as-prepared TiO$_2$ NTAs and mesoporous TiO$_2$-180 NTAs, (i) survey patterns,
(ii) F1s electron enlarged patterns

Considering that reactions between TiO_2 and F^- ions in the following chemical etching process may change the existing state of F^- ions on TiO_2 nanotubes, it is essential to study the state of F^- irons and make it clear whether F^- irons physically absorb on the surface or substitute in the crystal lattice of mesoporous TiO_2 NTAs. Fig.2 (ii) compares the XPS peaks of F1s electrons in high resolution between TiO_2 and mesoporous TiO_2-180 NTAs. F1s peak of mesoporous TiO_2 NTAs is a little higher than that of TiO_2 NTAs with the same binding energy, which is similar to the physically absorbed F^- on the surface of TiO_2 NTAs [34]. The similar state of F^- ions on TiO_2 NTAs before and after etching process confirms that F^- ions originate mainly from the anodization process.
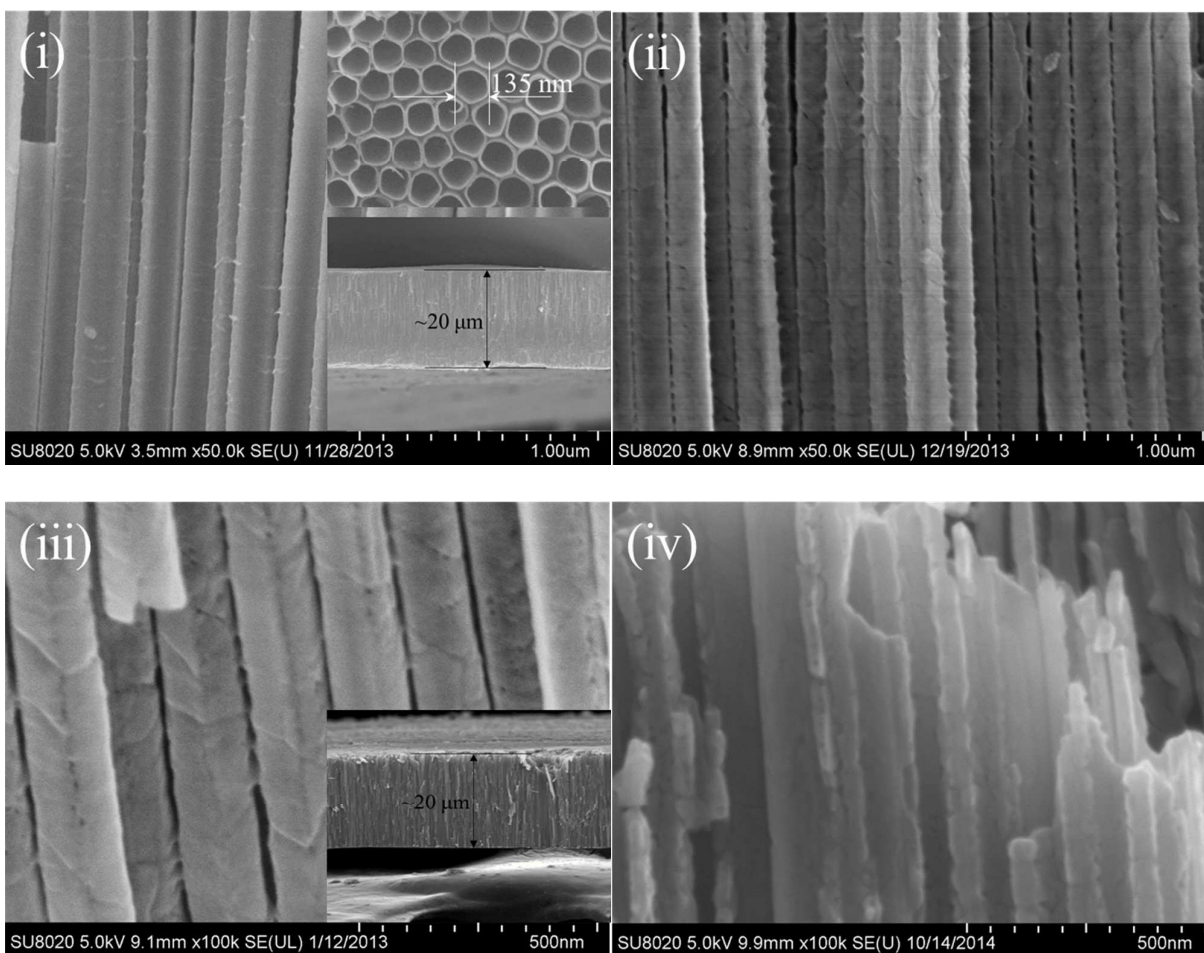

Fig.3 SEM morphologies of as-prepared TiO_2 (i), TiO_2-140 (ii), TiO_2-180 (iii) and TiO_2-200 (iv) NTAs

Fig.3 shows the SEM morphologies of as-prepared TiO_2 NTAs and mesoporous TiO_2 NTAs prepared at different etching temperatures. Well aligned TiO_2 NTAs with smooth tube walls can be observed in Fig.3 (i). Top-right inset is the top view of the nanotube arrays. These nanotubes are tightly aligned with a mean tube diameter of around 135 nm. Bottom-right inset is the general profile

view of TiO$_2$ NTAs, from which the tube length of approximate 20 μm can be obtained. Fig.3 (ii) shows the profile morphology of mesoporous TiO$_2$-140 NTAs. The well aligned structure of nanotubes still remains after being etched at 140℃. However, the smooth walls of TiO$_2$ nanotubes turns to be rough with observable etching trace. The interspace between the nanotubes appears after being treated in HF solution, indicating the etching effect of HF solution on the outside surface of nanotubes. When the etching temperature increase to 180℃, the etching trace becomes more evident than that of sample etched at 140℃, as shown in Fig.3 (iii). Bottom-right inset is the general profile view of TiO$_2$-180 NTAs, from which the tube length is almost the same with that of un-etched TiO$_2$ NTAs. Also, some through holes can be observed in the tube walls. Further increase of the etching temperature results in the evident destruction of the aligned structures, as shown in Fig.3 (iv). From the profile views of the broken nanotubes, many through holes in the tube walls can be observed. The penetration joints of the through holes lead to the destruction of the nanotubes.
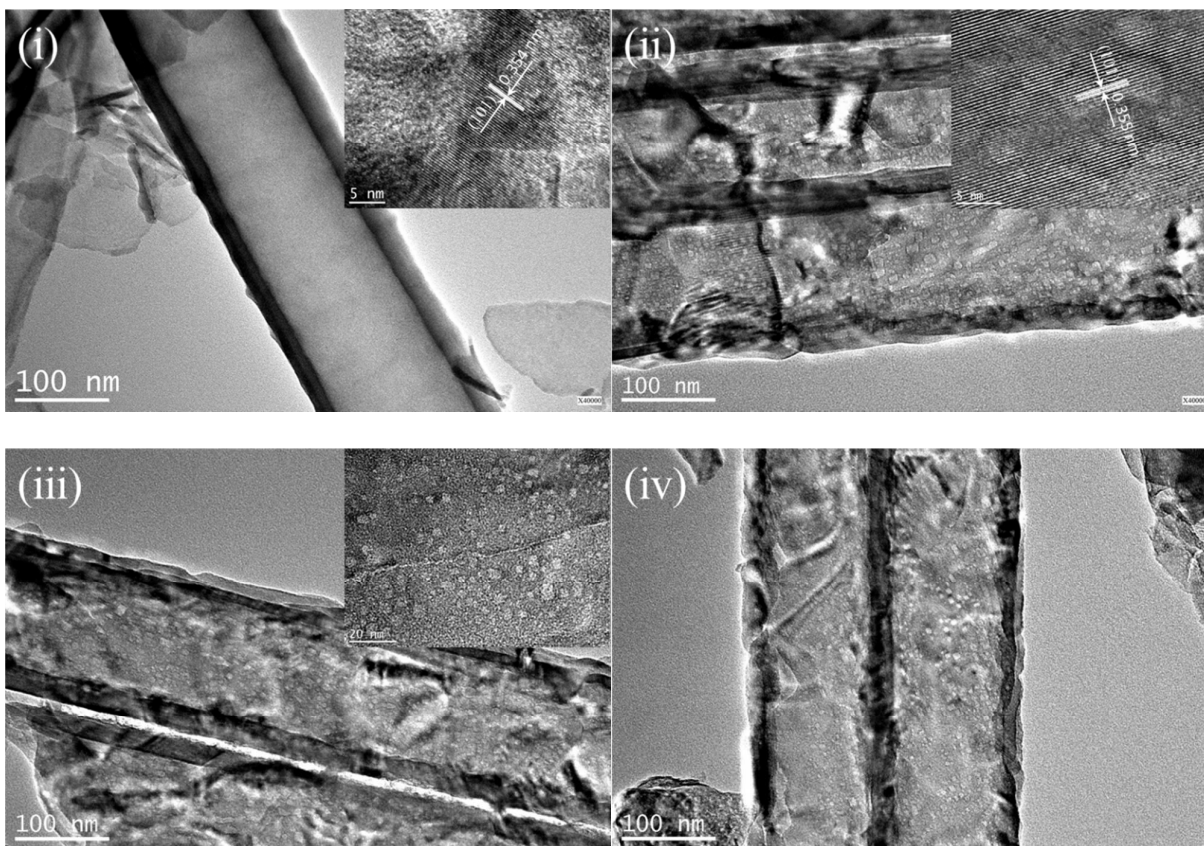

Fig.4 TEM morphologies of as-prepared TiO$_2$ (i), TiO$_2$-140 (ii), TiO$_2$-180 (iii) and TiO$_2$-200 (iv) NTAs, insets are the HRTEM morphologies of corresponding samples

Fig.4 shows TEM morphologies of as-prepared TiO$_2$ NTAs and mesoporous TiO$_2$ NTAs treated at

different temperatures. A nanotube with smooth surfaces both inside and outside can be observed in Fig.4 (i). Top-right inset is the HRTEM morphology of TiO$_2$ NTAs without further etching. The spacing of the lattice fringes measured to be 0.354 nm is consistent with the interplanar spacing of anatase (101) lattice planes, confirming the anatase structure of TiO$_2$ NTAs after being heat-treated. Compared with TiO$_2$ nanotubes in Fig.4 (i), there are lots of mesopores distributing in the inner walls of TiO$_2$ nanotubes after being etched at different temperatures, as shown in Fig.4 (ii), (iii) and (iv). And the size changes a little with the etching temperature increasing from 140 to 200℃. The clear edge of the tube walls can be observed in both TiO$_2$-140 and TiO$_2$-180 NTAs, although the surface is unsmooth. The roughness of the tube walls increases with the etching temperature, and even in TiO$_2$-200 NTAs, no evident edge of the tube wall can be observed due to the unsmooth surfaces. Top-right inset in Fig.4 (ii) shows the HRTEM morphology of TiO$_2$-140 NTAs. The same spacing of the lattice fringes indicates that the chemical etching process in HF solution doesn't change the crystal structure of TiO$_2$ NTAs. The polygonal mesopores with even size of around 5 nm in the tube walls can be observed in the top-right inset of Fig.4 (iii).

3.2 Photoelectrochemical properties

In order to achieve a maximum photocatalytic efficiency, the photogenerated electrons need to be separated from the holes. Applying a positive potential on the semiconductor were proven to be an effective way to move the electrons to the external circuit and achieve the chargers separation [35]. However, over-high positive potential may lead to direct electrochemical reactions which will distort the analytical signals and may even lead to false measurement [36].
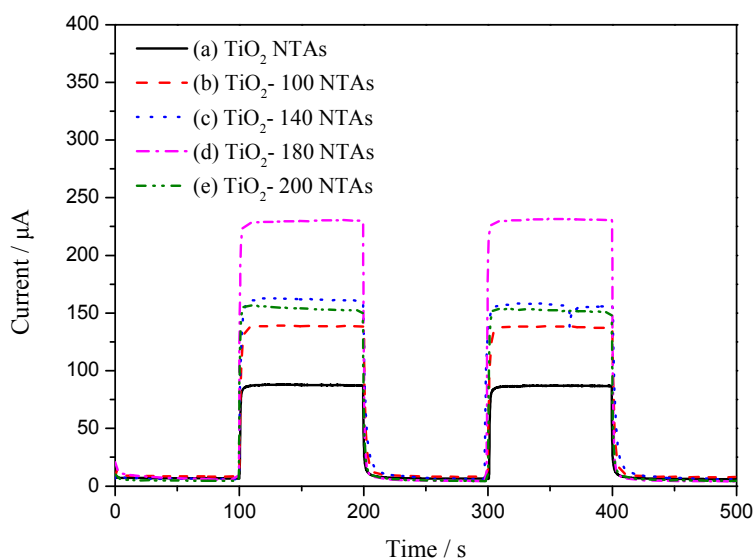

Fig.5 Photocurrent response of TiO$_2$ (a), TiO$_2$-100 (b), TiO$_2$-140 (c), TiO$_2$-180 (d) and TiO$_2$-200 (e)

NTAs in buffer solution, applied potential of 0.2 V, optical power output of 3%

Fig.5 shows the current-time curves of TiO$_2$ NTAs and mesoporous TiO$_2$ NTAs at the applied potential of 0.2 V. The UV light with optical power of 36 mW/cm^2 turns on and off at the elapse time of 100 s. The change of the current with light off and light on, as shown by solid line, gives the photocurrent produced by TiO$_2$ NTAs. The sharp increase and decrease of current with light on and light off due to the UV optical absorption and the formation of electron-hole pairs indicate the excellent photoelectrochemical activity of TiO$_2$ NTAs. Considering that the photoelectrochemical tests are conducted in phosphate buffer solution, the photocurrent originates from the optical water splitting. The photocurrent of as-prepared TiO$_2$ NTAs is 85.6 μA, and all the photocurrents of mesoporous TiO$_2$ NTAs are higher than that of as-prepared TiO$_2$ NTAs, indicating the effect of mesoporous structure on photocurrent. The photocurrent increases from 133 to 154.8 and 226.7 μA with the hydrothermal temperature from 100 to 140 and 180℃, respectively. Further increasing the temperature to 200℃ will decrease the photocurrent to 156.2 μA. The photocurrent of mesoporous TiO$_2$-180 NTAs achieves the maximum of 226.7 μA, which is almost 2.7 times that of un-etched TiO$_2$ NTAs.
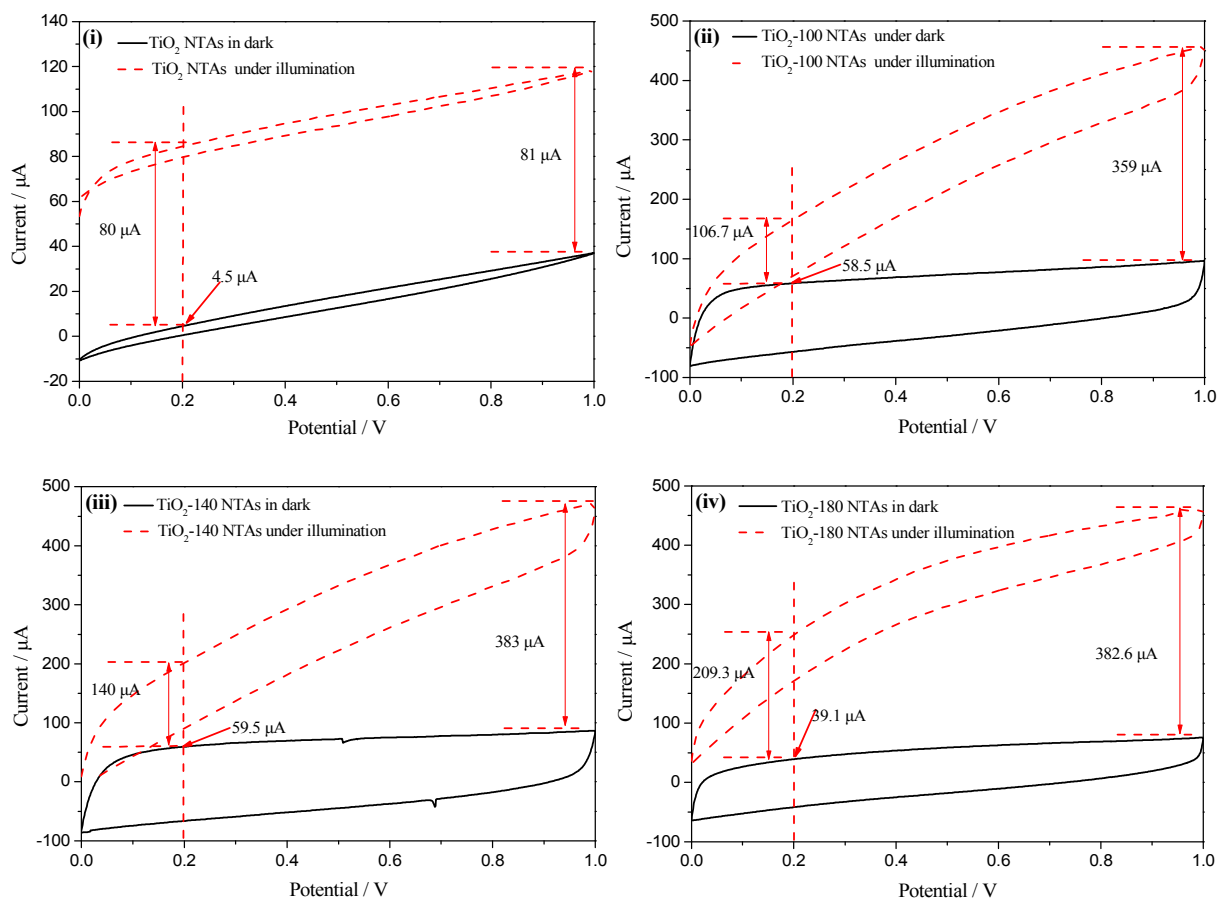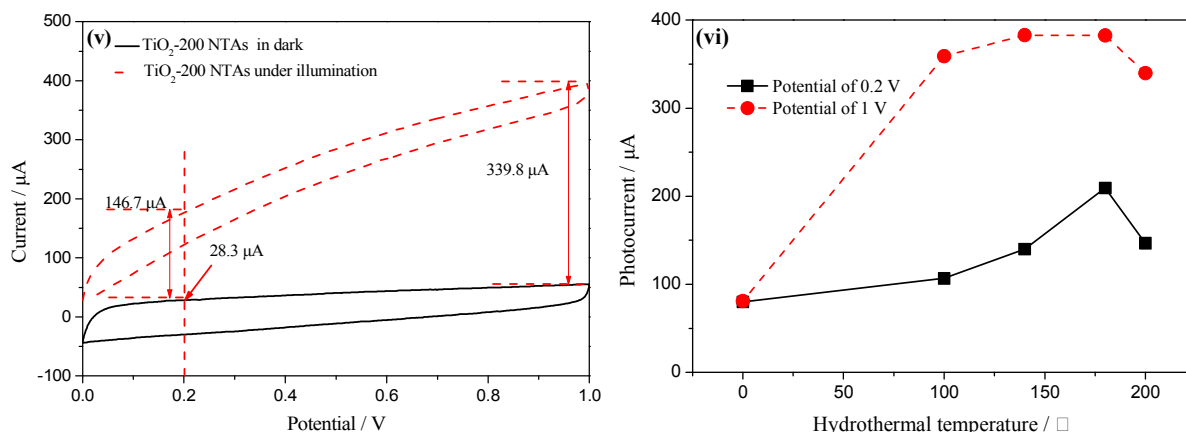
Fig.6 CVs of as-prepared TiO_2 (i); mesoporous TiO_2-100 (ii); TiO_2-140 (iii); TiO_2-180 (iv); TiO_2-200 (v) NTAs in dark and under illumination; (vi) plots of photocurrent vs. hydrothermal temperature at the potential of 0.2 and 0.7 V

Cyclic voltammetry is performed in different conditions to get the effect of bias potential on electrochemical and photoelectrochemical properties of as-prepared TiO_2 and mesoporous TiO_2 NTAs. Fig.6 shows cyclic voltammograms (CVs) of TiO_2 NTAs and mesoporous TiO_2 NTAs in dark and under illumination, respectively. The potential is ranging from 0 to 1 V and the sweeping rate is 0.01 V/s. The wavelength of UV light is 365 nm and the optical power is adjusted to be 36 mW/cm^2.

Fig.6 (i) shows the comparison of CVs obtained on TiO_2 NTAs in dark and under illumination respectively. When under illumination, the photocurrent increase quickly with the applied potential ranging from 0 to 0.1 V, then increase slowly with further increase of potential. The photocurrent is 80 μA at 0.2 V, and 81 μA at 1 V. The initial increase of the photocurrent at low applied potentials is due to the separation effect of applied potential on the photocurrent. When the applied potential is enough for complete separation of photogenerated electron/hole pairs, the photocurrent is under control of electron/hole pair productivity. Hence, further increasing applied potential cannot increase the photocurrent.

Fig.6 (ii), (iii), (iv) and (v) compare the CVs of mesoprous TiO_2 NTAs in dark and under illumination, respectively. All anodic currents in dark are higher than that of un-etched TiO_2 NTAs (4.5 μA), such as 58.5, 59.5, 39.1 and 28.3 μA at 0.2 V for TiO_2-100, TiO_2-140, TiO_2-180 and TiO_2-200 NTAs, respectively. Also, the photocurrents of mesoporous TiO_2 NTAs are higher than that of un-etched TiO_2 NTAs, fitting well with the results in Fig.5. The real data of photocurrent of TiO_2 NTAs vs. hydrothermal temperature at applied potentials of 0.2 and 1 V are shown in Fig.6 (vi). The square symbol with solid line shows the relationship between photocurrent and hydrothermal

temperature at the potential of 0.2 V. Photocurrent increases from 80 μA for un-etched TiO_2 NTAs to 106.7, 140 and 209.3 μA at the hydrothermal temperatures of 100, 140, and 180℃. Further increase of the temperature to 200℃ decreases the photocurrent to 146.7 μA. The sphere symbol with dash line shows the photocurrents at 0.7 V. Photocurrent increases from 81 μA for un-etched TiO_2 NTAs to 359, 383 and 382.6 μA for TiO_2-100, TiO_2-140 and TiO_2-180 NTAs, respectively. Also, the photocurrent decreases to 339.8 μA when hydrothermal temperature increases to 200℃.

The other thing should be noted is that the photocurrents of mesoporous TiO_2 NTAs increase with applied potential ranging from 0 to 1 V, such as 106.7 μA at 0.2 V and 359 μA at 1 V in TiO_2-100 NTAs, which is much different with that of un-etched TiO_2 NTAs. Electron/hole pair separation becomes the key factor for photocurrent due to the high electron/hole pair productivity in mesoporous TiO_2 NTAs. Low applied potential cannot separate the electron/hole pairs completely, and the separation efficiency of electron/hole pairs increases with increasing applied potential, manifesting as the increase of photocurrent.
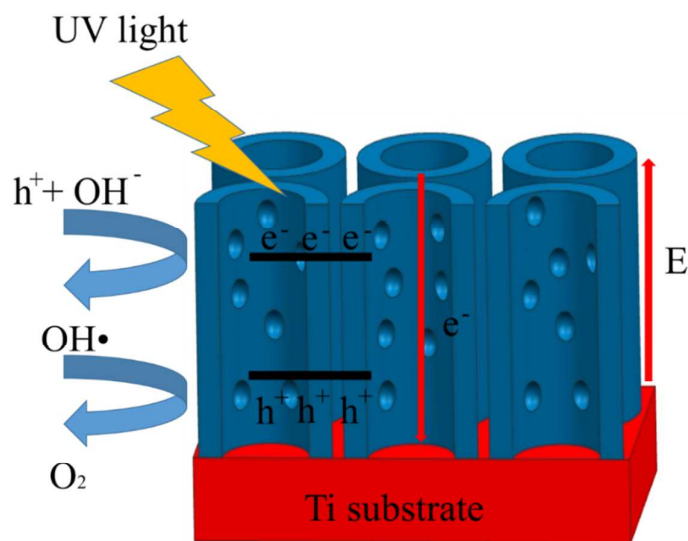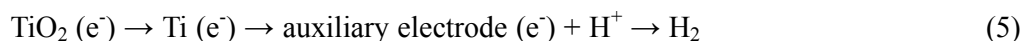
3.3 Mechanism discussion

Fig.7 Schematic diagram of photoelectrochemical process of mesoporous TiO_2 NTAs

The photoelectrochemical mechanism of TiO_2 NTAs can be described as the schematic diagram in Fig.7. The photoelectrochemical process of TiO_2 includes the generation of electron/hole pairs, electrons transfer to Ti substrate to form photocurrent in the external circuit, and holes transfer to the surface of catalyst forming oxidizing reactions. Mechanism of the photoelectrochemical process can be described as follows:

$$TiO_2 + hv \rightarrow TiO_2 \ (e^- + h^+) \tag{4}$$

$$TiO_2 \ (e^-) \rightarrow Ti \ (e^-) \rightarrow auxiliary \ electrode \ (e^-) + H^+ \rightarrow H_2 \tag{5}$$

$$TiO_2 \ (e^-) + TiO_2 \ (h^+) \rightarrow TiO_2 + hv^* \ (recombination) \tag{6}$$

$$TiO_2 \ (h^+) + OH^- \rightarrow HO\cdot \tag{7}$$

$$HO\cdot \ + \ HO\cdot \rightarrow O_2 \tag{8}$$

When TiO_2 captures a photon with an energy equal to or higher than the band gap, an electron (e^-) is promoted to the conduction band, leaving behind a positive hole (h^+) in the valence band, as shown in reaction (4). Photogenerated electrons and holes are separated by the applied electric field. Electrons transfer to back substrate and form photocurrent in the external circuit (Reaction (5)), accompanying with the recombination of electron/hole pairs (Reaction (6)). When the holes transfer to the surface of TiO_2 NTAs forming oxidizing reactions, the electrochemical active surface area obviously affects the reaction (7) and (8)

3.3.1 Optical absorption properties

The generation of electron/hole pairs under UV light illumination is the first step for photoelectrochemical process and a key factor for photoelectrochemical properties. Fig.8 shows the optical absorption patterns (i) and band gaps (ii) of as-prepared TiO_2 NTAs, mesoporous TiO_2-100, TiO_2-140, TiO_2-180 and TiO_2-200 (e) NTAs. TiO_2 NTAs possess excellent optical absorption in the UV region with an absorption edge at around 390 nm, corresponding to the band gap of anatase TiO_2. Mesoporous TiO_2 NTAs possess obviously enhanced optical absorption in the UV and visible region. At wavelength of 365 nm, the optical absorption intensity increases with the hydrothermal temperatures from 100℃ to 180℃, and achieves the maximum at 180℃. Further increase the temperature to 200℃ results the decrease of absorption intensity.
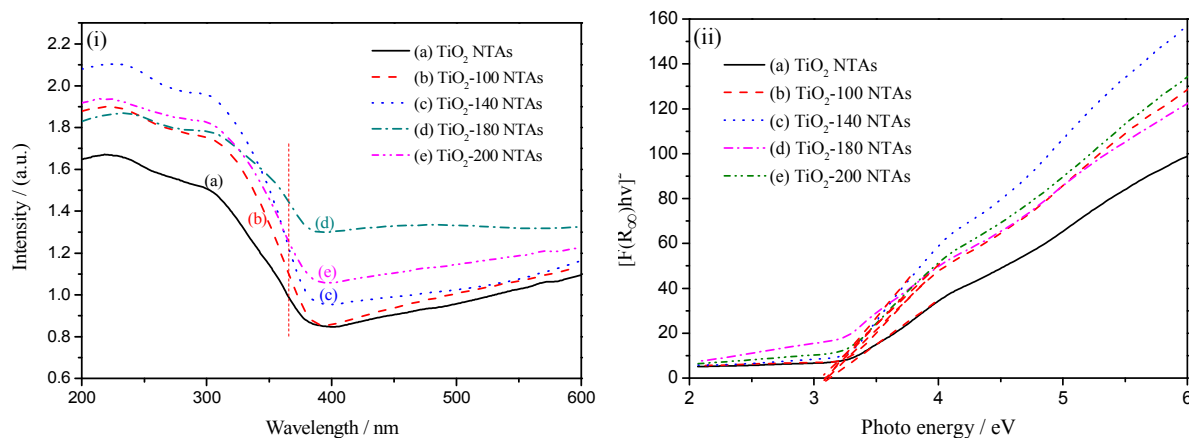
Fig.8 Optical absorption patterns (i) and band gaps (ii) of as-prepared TiO$_2$ NTAs, mesoporous TiO$_2$-100, TiO$_2$-140, TiO$_2$-180 and TiO$_2$-200 (e) NTA

The optical absorption is a complicated interaction between the light and substance, here including optical absorption and optical reflection. And a certain percentage of the light can be absorbed during each reflection process. The unsmooth surface induced by mesopores in the tube walls can increase the reflection times under illumination, which can enhance the optical absorption of TiO$_2$ NTAs.

The absorption changing law is in accordance with the changing law of photocurrent, indicating that high optical absorption is one of the main reasons for the high photocurrents in mesoporous TiO$_2$ NTAs. Thus, the relationship between photocurrent and applied potential, as being shown in Fig.6, can be explained as follows. Un-etched TiO$_2$ NTAs possess low optical absorption at 365 nm, which means electron/hole pairs productivity is low and becomes the limiting factor of photocurrent. These electron/hole pairs can be separated at low potentials effectively. Higher potential cannot enhance the photocurrent further due to the limitation of electron/hole pair productivity. However, mesoporous TiO$_2$ NTAs possess higher optical absorption properties than that of TiO$_2$ NTAs, indicating more electron/hole can be excited under UV illumination. The photogenerated electron/hole pairs can only be separated partially at low applied potentials, resulting in low photocurrents. Higher potentials promote the separation and decrease the recombination of electron/hole pairs and, hence increase the photocurrent.

In order to investigate whether chemical etching process influences the band gap of TiO$_2$ NTAs，band gaps of the TiO$_2$ and mesoporous TiO$_2$ NTAs are calculated according to the following Kubelka-Munk function:

$$F(R_\infty)=(1- R_\infty)^2/2\ R_\infty \tag{9}$$

Where R$_\infty$ is the diffuse reflectance. The extrapolation of a straight line to the photon energy axis (X axis) gives the band gap of TiO$_2$ and mesoporous TiO$_2$ NTAs, which are well consistent with the results of UV-vis absorption spectra. All samples show the similar band gaps at around 3.2 eV, indicating that the chemical etching process does not change the band gap of TiO$_2$ NTAs.

3.3.2 Charge transfer rate

Higher optical absorption of mesoporous TiO$_2$ NTAs would promote the reaction (Reaction 4) and produce more electron-hole pairs under UV illumination. However, it is different with photocatalytic process, in which the electrons participate the photocatalytic reactions through producing $\cdot O_2^-$ molecules, photogenerated electrons in the photoelectrochemical process go through the external

circuit forming photocurrent and are captured by H^+ ions on the auxiliary electrode (Reaction 5), except for recombination during the transfer process (Reaction 6). Electron transfer is a key factor affecting the photoelectrochemical performances.

In order to investigate the electrical conductivity of TiO_2 NTAs and mesoporous TiO_2 NTAs in buffer solution under illumination, the complex impedance analysis has been carried out in a traditional three electrode system. The electrochemical impedance measurement is conducted in a frequency range from 10^{-2} to 10^5 Hz at a potential of 0.1V under illumination. .

In general, the complex impendence is composed of charge transfer resistance in series with mass transfer impendence with linear and nonlinear diffusion terms. The semicircle part of the Nyquist plot gives the information about capacitance and resistance, the linear part shows the diffusion effects. The semicircle diameter at higher frequencies corresponds to the charge transfer resistance (R_{ct}), and the linear part at lower frequencies corresponds to the diffusion process.
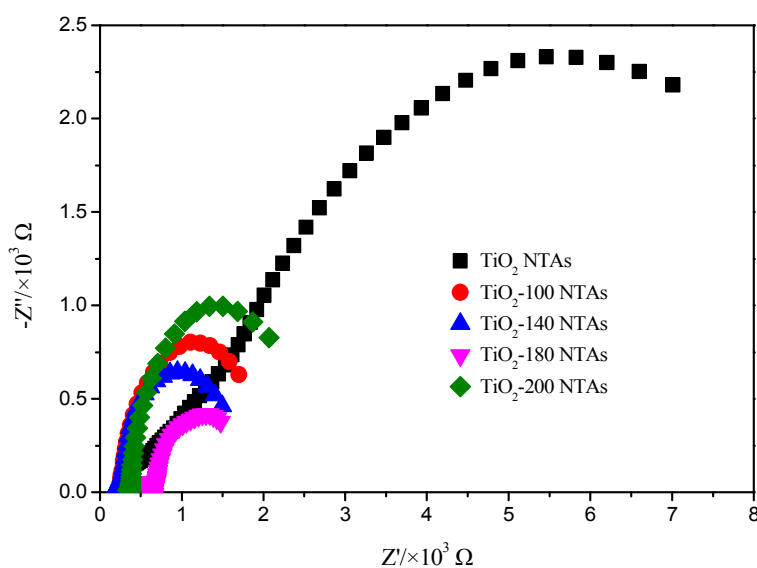

Fig.9 Nyquist plots of TiO_2, TiO_2-100, TiO_2-140, TiO_2-180 and TiO_2-200 NTAs under illumination in buffer solution

Fig.9 shows Nyquist plots of TiO_2 NTAs and mesoporous TiO_2 NTAs prepared at different temperatures. Compared with TiO_2 NTAs, obvious descent of semicircle radiuses can be observed, indicating the low charge transfer resistance of mesoporous TiO_2 NTAs. The R_{ct} of mesoporous TiO_2 NTAs decreases with the hydrothermal temperature increasing from 100 to 180℃, and achieves the lowest R_{ct} at temperature of 180℃, indicating the highest electron transfer rate. Further increase the hydrothermal temperature to 200℃, the transfer rate decrease, which may be due to the destruction

of TiO$_2$ NTAs structures.

The charger transfer rate is influenced by two factors including and the intrinsic impedance of TiO$_2$ nanotubes and interfacial resistance between TiO$_2$ and the electrolyte. Constructing mesopores in TiO$_2$ tube walls can decrease the interfacial impedance rather than the intrinsic impedance, hence increase the charger transfer rate.

3.3.3 Electrochemical active surface area

Fig.10 shows typical CVs of as-prepared TiO$_2$ and mesoporous TiO$_2$ NTAs in the electrolyte containing 10 mM K$_3$[Fe(CN)$_6$] and 0.1 M KCl, which can characterize the electrochemical active surface of the electrode. A pair of redox peaks can be observed on TiO$_2$ NTAs at the potentials ranging from 0 to 0.6 V due to the oxidation and reduction of [Fe(CN)$_6$]$^{3-}$ ions.
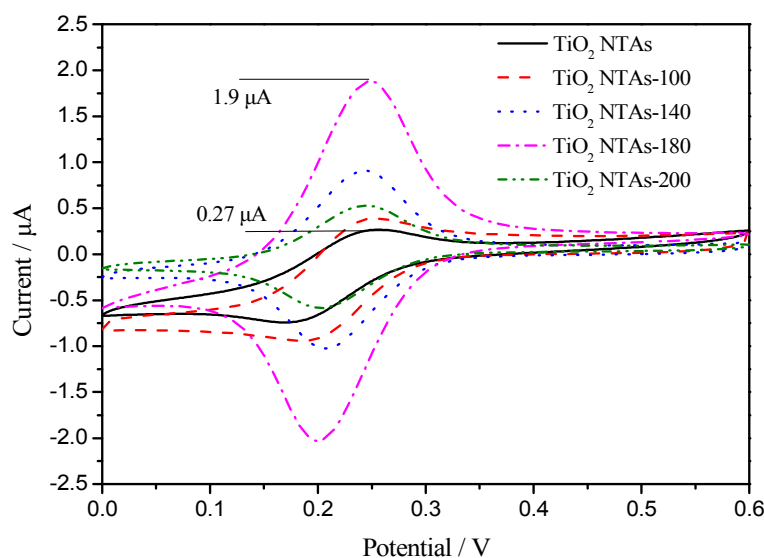

Fig.10 CVs of as-prepared TiO$_2$, TiO$_2$-100, TiO$_2$-140, TiO$_2$-180 and TiO$_2$-200 NTAs in an aqueous solution containing 10 mM K$_3$[Fe(CN)$_6$] and 0.1 M KCl

For a reversible process, Randles-Sevick Equation is applicable. Therefore, the electrochemical active surface areas of TiO$_2$ NTAs and mesoporous TiO$_2$ NTAs can be determined by equation (10).

$$I_P = (2.69 \times 10^5) n^{3/2} A D_0^{1/2} v^{1/2} C_0^* \tag{10}$$

Where I_P is the peak current, n is the number of electrodes, A is the electrochemical active surface area of the electrode (in cm^2), C_0^* is the concentration (in mol/cm^3), D_0 is the diffusion coefficient (in cm^2/s) and v is the scan rate (in V/s). The peak current (I_p) corresponds to the electrochemical active surface area (A) of the electrodes.

15

All mesoporous TiO_2 NTAs exhibit higher peak intensities and larger capacitance than that of as-prepared TiO_2 NTAs, indicating that mesoporous TiO_2 NTAs possess larger electrochemical active surface areas. The peak current increases with hydrothermal temperature ranging from 100℃ to 180℃ and achieves the maximum of 1.9 μA at the temperature of 180℃. Further increase of the temperature to 200℃ decreases the peak current to 0.9 μA. The change of peak currents corresponds to the change of the electrochemical active surface area, that is, the mesoporous TiO_2-180 NTAs possess the biggest electrochemical active surface area.

4 Conclusions

In this work, mesoporous TiO_2 nanotube arrays are successfully synthesized by chemical etching in HF solution. Effect of hydrothermal temperature on the mesoporous structure and photoelectrochemical activities are also discussed. Mesopores with a rectangular shape mainly distribute in the inner walls of TiO_2 nanotube. The mesoporous TiO_2 nanotube arrays possess better photoelectrochemical properties than that of as-prepared TiO_2 nanotube arrays, and the TiO_2-180 nanotube arrays achieves the highest photocurrent. Moreover, the photocurrent of mesoporous TiO_2 are sensitive to the applied potential ranging from 0 to 1 V due to the high electron/hole pair productivity. The photoelectrochemical mechanism of the mesoporous TiO_2 nanotube arrays is discussed from the whole photoelectrochemical process. The introduction of mesopores in TiO_2 nanotubes enhances the optical absorption, increases the electrochemical active surface area and facilitates the charge transfer at the same time. Thus, the mesoporous TiO_2 nanotube arrays possess better photoelectrochemical properties than that of un-etched TiO_2 nanotube arrays.

Acknowledgements

References

[1] A. Fujishima, K. Honda, Nature, 238 (1972) 37-38

[2] A. Fujishima, Tata N. Rao, Donald A. Tryk, T, J. photochem. Photobio. C, Photochemistry Reviews, 1 (2000) 1-21

[3] Xiaobo Chen, Samuel S. Mao, Chem. Rev., 107 (2007) 2891-2959

[4] Gopal K. Mor, Karthik Shankar, Maggie Paulose, Oommen K. Varghese, Craig A. Grimes, Nano Lett., 2 (2006) 215-218

[5] Kai Zhu, Nathan R. Neale, Alexander Miedaner, Arthur J. Frank, Nano Lett., 7 (2007) 69-74

[6] U. Bach, D. Lupo, P. Comte, J. E. Moser, F. Weissorted, J. Salbeek, H. Spreitzer, Nature, 395 (1998) 583-685

[7] Andrei Ghicov, Masahiro Yamamoto, Patrik Schmuki, Angew. Chem., 120 (2008) 8052-8055

[8] Donghai Wang, Daiwan Choi, Juan Li, Zhengua Yang, Zimin Nie, Nano, 3 (2009) 907-914

[9] Hui Xiong, Michael D. Slater, Mahalingam Balasubramanian, J. Phy. Chem. Lett., 2 (2001) 2560-2565

[10] Shu-Juan Bao, Chang Ming Li, Jian-Feng Zang, Xiao-Qiang Cui, Adv. Funct. Materi., 18 (2008) 591-599

[11] Gopal K. Mor, Maria A. Carvacho, Ooman K. Varghese, Michael V. Pishko, J. Mater. Res., 19 (2004) 628-634

[12] Shenglian Luo, Fang Su, Chengbin Liu, Juanxiu Li, Ronghua Liu, Talanta, 86 (2011) 157-163

[13] V. Zwilling, M. Aucouturier, E. Darque-Ceretti, Electrochim. Acta., 45 (1999) 921-929

[14] Thillai Sivakumar Natarajan, Kalithasan Natarajan, Hari C. Bajaj, Rajesh J. Tayade, Ind. Eng. Chem. Res., 50 (2011) 7753-7762

[15] Haimin Zhang, Porun Liu, Xiaolu Liu, Shangqing Zhang, Xiaodong Yao, Langmuir, 26 (2010) 11226-11232

[16] Qing Zheng, Baoxue Zhou, Jing Bai, Longhai Li, Zhujing Jin, Jialing Zhang, Adv. Mater., 20 (2008) 1044-1049

[17] Gregorio F. Ortiz, Ilie Hanzu, Thierry Djenizian, Pedro Lavela, Chem. Mater., 21 (2009) 63-67

[18] Wenxi Guo, Xinyu Xue, Sihang Wang, Changjian Lin, Nano Lett., 12 (2012) 2520-2523

[19] Qing Liu Wu, Juchuan Li, Rutooj D. Deshpande, Navaladian Subramanian, J. Phy. Chem. C, 116 (2012) 18669-18667

[20] Xinjian Feng, Jennifer D. Sloppy, Thomas J. LaTempa, Maggie Paulose, Sridhar Komarnemi, J. Mater. Chem., 21 (2011) 13429-13433

[21] Jong Hyeok Park, Sungwook Kim, Allen J. Bard, Nano Lett., 6 (2006) 24-28

[22] Zhonghai Zhang, Md. Faruk Hossain, Takakazu Takahashi, Int. J. Hydrogen Energ., 35 (2010) 8528-8535

[23] Naser Alenzi, Wei-Ssu Liao, Paul S. Cremer, Viviana Sanchez-Torres, Int. J. Hydrogen Energ., 35 (2010) 11768-11775

[24] Jiaguo Yu, Lifang Qi, Mietek Jaroniec, J. Phy. Chem. C, 114 (2010) 13118-13125

[25] Caolong Li, Jian Yuan, Bingyan Han, Li Jiang, Int. J. Hydrogen Energ., 36 (2010) 7073-7079

[26] Yuh-lang Lee, Ching-Fa Chi, Shih-Yi Liau, Chem. Mater., 22 (2010) 922-927

[27] Quanjun Xiang, Jiaguo Yu, Mietek Jaroniee, J. Am. Chem. Soc., 134 (2012) 6575-6578

[28] Chen, J. S., Tan, Y. L., Li, C. M., Cheah, Y. L., Luan, D., Madhavi, J. Am. Chem. Soc., 132 (2010) 6124-6130

[29] S.J. Bao, Q.L. Bao, C.M. Li, Z.L. Dong, Electrochem. Commun., 9 (2007) 1233-1238

[30] S.J. Bao, C.M. Li, J.F. Zang, X.Q. Cui, Y. Qiao, J. Guo, Adv. Funct. Mater., 18 (2008) 591-599

[31] Jaturong Jitputti, Sorapong Pavasupree, Yoshikavu Suzuki, J. Solid State Chem., 180 (2007) 1743-1749

[32] Pascal Hartmann, Doh-kwon Lee, Bernd M. Smarsly, Juergen Janek, Nano, 4 (2010) 3147-3154

[33] Lihang Li, Min Yang, Shanqing Zhang, Nanotechnology, 21 (2010) 485503-485512

[34] Guosheng Wu, Jingpeng Wang, Dan F. Thomas, Archeng Chen, Langmuir, 24 (2008) 3503-3509

[35] Dianlu Jiang, Huijun Zhao, Shanqing Zhang, J. Phy. Chem. B, 107 (2003) 12774-12782

[36] Yanhe Han, Jingxia Qiu, Yuqing Miao, Shanqing Zhang, Anal. Method., 3 (2011) 2003-2009
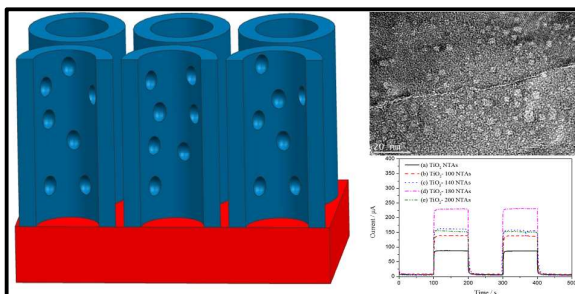
Mesopores are etched in the tube walls of TiO_2 nanotubes, which can enhance the photoelectrochemical activities of TiO_2 NTAs.